

# SIJMJ7 orchestrates tomato fruit ripening via crosstalk between H3K4me3 and DML2-mediated DNA demethylation

Xiaochun Ding<sup>1\*</sup>, Xuncheng Liu<sup>1,2\*</sup> , Guoxiang Jiang<sup>1</sup>, Zhiwei Li<sup>1,3</sup>, Yunbo Song<sup>1</sup>, Dandan Zhang<sup>1</sup>, Yueming Jiang<sup>1,2,4</sup>  and Xuewu Duan<sup>1,2,4,5</sup> 

<sup>1</sup>Guangdong Provincial Key Laboratory of Applied Botany, South China Botanical Garden, Chinese Academy of Sciences, Guangzhou 510650, China; <sup>2</sup>Center of Economic Botany, Core Botanical Gardens, Chinese Academy of Sciences, Guangzhou 510650, China; <sup>3</sup>College of Life Sciences, University of Chinese Academy of Sciences, Beijing 100049, China; <sup>4</sup>College of Advanced Agricultural Sciences, University of Chinese Academy of Sciences, Beijing 10049, China; <sup>5</sup>Agro-food Science and Technology Research Institute, Guangxi Academy of Agricultural Sciences, Nanning 530007, China

## Summary

Authors for correspondence:  
Xuewu Duan  
Email: xwduan@scbg.ac.cn

Yueming Jiang  
Email: ymjjiang@scbg.ac.cn

Received: 20 July 2021  
Accepted: 28 October 2021

*New Phytologist* (2022) **233**: 1202–1219  
doi: 10.1111/nph.17838

**Key words:** DML2, DNA demethylation, epigenetic interaction, fruit ripening, histone demethylase, histone demethylation, tomato.

- The ripening of fleshy fruits is a unique developmental process that Arabidopsis and rice lack. This process is driven by hormones and transcription factors. However, the critical and early regulators of fruit ripening are still poorly understood.
- Here, we revealed that SIJMJ7, an H3K4 demethylase, is a critical negative regulator of fruit ripening in tomato.
- Combined genome-wide transcription, binding sites, histone H3K4me3 and DNA methylation analyses demonstrated that SIJMJ7 regulates a key group of ripening-related genes, including ethylene biosynthesis (*ACS2*, *ACS4* and *ACO6*), transcriptional regulation (*RIN* and *NOR*) and DNA demethylation (*DML2*) genes, by H3K4me3 demethylation. Moreover, loss of *SIJMJ7* function leads to increased H3K4me3 levels, which directly activates ripening-related genes, and to global *DML2*-mediated DNA hypomethylation in fruit, which indirectly prompts expression of ripening-related genes. Together, these effects lead to accelerated fruit ripening in *sljmj7* mutant.
- Our findings demonstrate that SIJMJ7 acts as a master negative regulator of fruit ripening not only through direct removal of H3K4me3 from multiple key ripening-related factors, but also through crosstalk between histone and DNA demethylation. These findings reveal a novel crosstalk between histone methylation and DNA methylation to regulate gene expression in plant developmental processes.

## Introduction

Fleshy fruits represent an important food source for humans. The ripening of fleshy fruits is a unique developmental process that Arabidopsis and rice lack, involving dramatic changes in color, texture, flavor and nutrition. Fruit ripening usually commences after growth ceases. The ripening process is controlled by a complex network of endogenous factors and exogenous cues (Seymour *et al.*, 2013), and unraveling its regulatory network is therefore important for developing strategies to improve nutritional and sensory qualities (Giovannoni *et al.*, 2017).

Tomato has been used as a model system to study the mechanism underlying the regulation of fruit ripening because of relative ease of genetic transformation, short life cycle and well-annotated genome (Giovannoni *et al.*, 2017). The plant hormone ethylene is considered the main trigger of the tomato ripening process. Ethylene is biosynthesized by two key enzymes, aminocyclopropane-1-carboxylate (ACC) synthase (ACS) and ACC oxidase (ACO), and initiates ripening-related transcriptional responses via a series of

signal transduction processes (Gray *et al.*, 1994). The complex regulatory network of tomato fruit ripening has been well characterized. Several transcription factors, such as RIN, NOR and CNR, have been identified as the major regulators that regulate fruit ripening in concert with ethylene signaling (Thompson *et al.*, 1999; Vrebalov *et al.*, 2002; Manning *et al.*, 2006).

In addition, DNA methylation, a conserved epigenetic modification generally associated with transcriptional inactivation (Law & Jacobsen, 2010; He *et al.*, 2011), has been found to be essential for tomato fruit ripening (Zhong *et al.*, 2013). In tomato, repression or loss of function of the DEMETER-like DNA demethylase *DML2* has been shown to result in DNA hypermethylation and inhibition of ripening (Liu *et al.*, 2015; Lang *et al.*, 2017). Moreover, *DML2* activates the demethylation of the *RIN*, *NOR* and *CNR* promoter regions, thereby allowing these gene expressions (Liu *et al.*, 2015). Yet, despite it being known that tomato fruit ripening is controlled by the complex roles of ethylene, ripening-related transcription factors and *DML2*-mediated DNA demethylation, it is unknown whether other types of epigenetic modifications play a role in this process.

\*These authors contributed equally to this work.

Histone lysine methylation is another type of epigenetic modification, which mainly occurs at K4, K9, K27 and K36 of histone H3. In general, H3K27 and H3K9 histone methylation are related to inactive chromatin and gene silencing, whereas H3K4 and H3K36 methylation are associated with gene activation (Kouzarides, 2007). These marks are written by histone methyltransferases and erased by histone demethylases (Liu *et al.*, 2010). Two types of enzymes with distinct mechanisms, lysine-specific demethylase 1 (LSD1) and Jumonji C (JmjC) domain-containing proteins (JMJs), have been identified to be erasers of histone methylation (Shi *et al.*, 2004; Tsukada *et al.*, 2006; Lu *et al.*, 2008). LSD1 family proteins acts only mono- and dimethylated lysine, and JMJs have demethylase activities towards to mono-, di- and trimethylated lysine. Histone demethylases have been extensively studied in the model plants *Arabidopsis* and rice. In *Arabidopsis*, AtJMJs (AtJM11–AtJM31) represent the majority of histone demethylase and play essential roles in the regulation of seed dormancy/germination, organ morphogenesis, vegetative development and floral transition as well as in abiotic stress responses (Cheng *et al.*, 2020). Recent works reported a critical role of the repressive mark H3K27me<sub>3</sub> in the regulation of fruit ripening (Liang *et al.*, 2020; Z. Li *et al.*, 2020), and that SIJM7, a histone H3K27me<sub>2/3</sub> demethylase, promotes tomato fruit ripening by activating ripening-related genes (Z. Li *et al.*, 2020). However, the role of H3K4, an activation mark, in the regulation of fleshy fruit ripening and the underlying mechanism in relation to the interplay among epigenetic modifications remains unclear.

Our preliminary results showed that SIJM7, a KDM5/JARIDA1-type JMJ, has histone H3K4 demethylase activity, and the transcription level of *SIJM7* was enormously upregulated and then decreased during fruit ripening in tomato. We hypothesized that SIJM7-mediated histone H3K4 demethylation is implicated in the regulation of fruit ripening in tomato. Here, we identified that SIJM7 acts as a repressor of fruit ripening in tomato. SIJM7 was confirmed to specifically demethylate mono-, di- and trimethylated lysine of H3K4 and to directly repress expression of *DML2*, leading to global DNA hypermethylation in tomato fruit. Moreover, combined genome-wide transcription, binding sites, histone modification and DNA methylation profile analyses revealed that SIJM7 integrates the transcriptional regulators, ethylene biosynthesis and other ripening-related factors with H3K4me<sub>3</sub> and DNA demethylation to regulate fruit ripening. Our study of fruit ripening reveals a novel molecular link between histone demethylation and DNA demethylation.

## Materials and Methods

### Plant material and growth conditions

The tomato plants used in this study were in the Ailsa Craig background and grown in a glasshouse at 23°C under a 16 h : 8 h, light : dark cycle. Flowers were tagged at anthesis. Fruit development and ripening stages were recorded as days post-anthesis (dpa). Pericarp tissues of the fruits were collected, immediately frozen in liquid nitrogen and stored at –80°C until use.

### Construction of *SIJM7* overexpression lines and *slj mj7* mutants

*SIJM7* cDNA was isolated using gene-specific primers and cloned into a pBI121-GFP vector (p35S: GFP). pBI121-SIJM7-GFP vector was transformed into wild-type (WT) plants by *Agrobacterium*-mediated (GV3101) infection as described previously (Fillatti *et al.*, 1987). The transgenic lines were selected for kanamycin resistance. To generate *slj mj7* knockout mutants, two *SIJM7*-specific targets were designed using the online CRISPR 2.0 program (<http://cbi.hzau.edu.cn/CRISPR2/>) (Liu *et al.*, 2017). The fragment containing the first *BsaI* site, sgRNA1, tRNA, sgRNA2 and the second *BsaI* site were amplified from tRNA vector (pHLW-sgRNA-tRNA) using primers (sgRNA1 primer, GAATCAGCAATATGGAGTCCTGG; sgRNA2 primer, TACCA TATTTCTGTGCGTTGTGG), and then inserted into the linearized Cas9 binary vector (pPTG-sgRNA-Cas9-AtU6-1) as previously described (Wang *et al.*, 2018). The Cas9 binary vector was provided by Dr Yifei Liu (South China Botanical Garden, CAS). The construct was then transformed into WT plants using the method described earlier. The mutated genomic sites in the transgenic plant genome were amplified by PCR and confirmed by Sanger sequencing. The primer pairs used for vector construction and mutational analyses are listed in Supporting Information Dataset S1.

### Measurement of physiological parameters

To measure ethylene production, five fruits were sealed in a 500 ml container for 2 h at 25°C. One milliliter of headspace gas was withdrawn and analyzed using a Hewlett-Packard 5890 series gas chromatograph equipped with a 25 m HP-PLOT Q capillary column (Agilent Technologies, Santa Clara, CA, USA) and a flame ionization detector. The chlorophyll *a/b* contents were measured using a UV1800 spectrophotometer (Shimadzu, Kyoto, Japan). Carotenoids from tomato pericarp were extracted as previously described (Xu *et al.*, 2006). In brief, 300 mg of pericarp tissue was ground in liquid nitrogen and extracted in 250 µl of methanol, 500 of chloroform and 250 µl of 50 mM Tris-buffer (pH 7.5, containing 1 M NaCl). After centrifugation, the chloroform phase was collected and dried under a stream of nitrogen. The residue was dissolved in 100 µl methanol and analyzed by high-performance liquid chromatography with a Waters Symmetry Shield RP18 reverse-phase column (4.6 × 250 mm × 5 µm) as previously described (Zheng *et al.*, 2015).

### Histone demethylation assay

Two assays were performed to determine the histone demethylation activity of SIJM7. The *in vivo* histone demethylation assay was performed as previously described (Lu *et al.*, 2011). In brief, pBI121-35S-SIJM7-GFP and pBI121-35S-SIJM7<sup>H288A/E290A</sup>-GFP mutant recombinant vectors were transformed into *Agrobacterium tumefaciens* (GV3101) and then transfected into *Nicotiana benthamiana* leaves. The infiltrated leaves were used for isolation of nuclei, and immunostaining was then

performed with anti-histone methylation-specific antibodies (listed later) followed by detection with Alexa Fluor 568-conjugated goat anti-rabbit (Invitrogen) secondary antibodies. Nuclear localization was visualized using 4',6-diamidino-2-phenylindole (DAPI) staining. The fluorescence signals were observed and images were acquired under a laser confocal microscope (Leica, Wetzlar, Germany) at  $\times 40$  magnifications. For Western blot analysis, histones were extracted from the leaves of WT and transgenic plants using a Total Histone Extraction Kit (Epigentek, Farmingdale, NY, USA). The antibodies used in the histone demethylation assay were as follows: anti-H3 (ab1791; Abcam, Cambridge, MA, USA), anti-H3K4me1 (A2355; ABclonal, Wuhan, China), anti-H3K4me2 (07-030; Millipore, Darmstadt, Germany), anti-H3K4me3 (07-473; Millipore), anti-H3K9me1 (A2358; ABclonal), anti-H3K9me2 (07-441; Millipore), anti-H3K9me3 (07-442; Millipore), anti-H3K27me1 (A2361; ABclonal), anti-H3K27me2 (07-452; Millipore), anti-H3K27me3 (07-449; Millipore), anti-H3K36me1 (A2354; ABclonal), anti-H3K36me2 (ab9049; Abcam) and anti-H3K36me3 (ab9050; Abcam). For *in vitro* demethylation assay, SIJM7-GFP was immunoaffinity-purified from transiently expressing tobacco leaves. The demethylation assay was carried out as previously described with minor modifications (D. Li *et al.*, 2020). In brief, enzyme and calf thymus histones (Sigma H9250) were incubated in reaction buffer (150 mM NaCl, 20 mM HEPES-NaOH, 50  $\mu$ M Fe(NH<sub>4</sub>)<sub>2</sub>(SO<sub>4</sub>)<sub>2</sub>, 1 mM  $\alpha$ -ketoglutarate, 2 mM ascorbate, pH 8.0) for 6 h at 30°C. Then the reaction product was analyzed by Western blot using the antibodies mentioned earlier.

### Western blot

Protein extracts were separated on 15% sodium dodecyl sulfate-polyacrylamide gel electrophoresis gels and transferred to polyvinylidene difluoride (PVDF) membranes blocked in 5% bovine serum albumin overnight at 4°C. Primary antibody was added at a ratio of 1 : 1000 and incubated overnight at 4°C. The PVDF was washed three times with Tris-buffered saline with 0.1% Tween-20 for 15 min each time. Secondary antibody was added at a ratio of 1 : 5000 and incubated for 2–3 h at room temperature. After washing three times with Tris-buffered saline plus Tween-20, the membranes are visualized using ChemiDoc Touch Imaging System (Bio-Rad Hercules, CA, USA).

### Real-time quantitative PCR assay

Total RNA was extracted using the HiPure Plant RNA Mini kit (Magen, Guangzhou, China), followed by reverse transcription. The first-strand cDNA was used for real-time quantitative polymerase chain reaction (RT-qPCR) in the ABI7500 Real-Time PCR System (Thermo Fisher Scientific, Waltham, MA, USA) using a THUNDERBIRD™ SYBR™ qPCR Mix (Toyobo, Osaka, Japan). *ACTIN* (*Solyc03g078400*) was used as the internal control. All RT-qPCRs were normalized using the  $C_t$  value corresponding to the reference gene. The relative expression levels were calculated with the formula  $2^{-\Delta\Delta C_t}$ . Three independent

biological replicates were used in the analysis. The primers used for RT-qPCR analysis are listed in Dataset S1.

### RNA-seq analysis

Total RNA isolated from *sljnj7-1* and WT fruits at 38 dpa was extracted using the HiPure Plant RNA Mini kit (Magen). The mRNA-seq library was constructed using the mRNA-Seq Kit (Illumina, San Diego, CA, USA) and then sequenced on Illumina HiSeq 2500 by Novogene Co. (Beijing, China), with three independent biological replicates. The low-quality reads with > 10% unknown nucleotides and the percentage of Q-value ( $\leq 20$ ) base > 50% were filtered out. The clean reads were aligned to the tomato genome (SL3.0) using HISAT2 (v.2.0.1) with the default parameters. HTSEQ v.6.0 was used to count the reads numbers mapped to each gene, and fragments per kilobase of exon model per million mapped fragments (FPKM) was used to estimate gene expression levels. The differentially expressed genes were identified using DESeq, with an absolute value of  $\log_2$ (fold change) (*sljnj7* vs WT)  $\geq 1$  and an adjusted *P*-value (false discovery rate (FDR)) < 0.05 set as the threshold criteria. Gene functional classification was carried out with the DAVID functional annotation clustering tool (<https://david.ncifcrf.gov/gene2gene.jsp>) (Huang *et al.*, 2009).

### Chromatin immunoprecipitation sequencing analysis

Tomato pericarp tissue was fixed in 1  $\times$  phosphate-buffered saline containing 1% formaldehyde. Nuclei were purified using one-step Percoll gradient centrifugation. Chromatin DNA was sonicated with a Sonic Dismembrator (Thermo Fisher Scientific) to generate fragments of 300–500 bp. Anti-H3K4me3 and anti-GFP antibodies (ab290, Abcam) were used for immunoprecipitation as previously described (Ricardi *et al.*, 2010). The immunoprecipitated DNA was used for chromatin immunoprecipitation sequencing (ChIP-seq) DNA library preparation using a NEBNext DNA Library Prep Master Mix Set for Illumina. All the libraries were sequenced on the Illumina HiSeq X Ten platform in PE150 mode. Three biological replicates were prepared for each line. The clean reads were mapped to SL3.0 using BOWTIE2 (v.2.2.3) (<http://bowtie-bio.sourceforge.net/bowtie2/index>). Differential enrichment was assessed with MACS2, HOMER and DESEQ2 with an FDR cut-off of < 0.001. The regions with differential histone modification were intersected with the annotated genes to obtain the target genes using BEDTOOLS. The alignments were converted to wiggle (WIG) files. The data were then imported into the Integrated Genome Browser for visualization.

### ChIP-qPCR assay

Chromatin immunoprecipitation (ChIP)-qPCR assays were performed as previously described (Gendrel *et al.*, 2005). Briefly, the chromatin in tomato samples was sonicated into fragments with an average length of 500 bp; 10% of the sonicated chromatin was used as the input control, and 90% was immunoprecipitated with equal amounts of antibodies, including

anti-H3K4me3, anti-GFP and anti-SIJMJ7 (anti-KDM5C, ab34718; Abcam; herein referred to as anti-SIJMJ7) antibodies, and anti-immunoglobulin G (ab231712; Abcam). The abundance of immunoprecipitated chromatin was determined by RT-qPCR using the primers listed in Dataset S1. Three biological replicates were analyzed per line.

### Whole-genome bisulfite sequencing

Whole-genome bisulfite sequencing (WGBS) was performed as previously described (H. Huang *et al.*, 2019; S. Huang *et al.*, 2019). Genomic DNA extracted from tomato pericarp was fragmented to an average size of 300–500 bp. Fragmented DNA was end-repaired and ligated to a fully methylated adapter using a NEXTflex Bisulfite-Seq Barcodes-6 Kit (51191; Bioo Scientific, Austin, TX, USA). After bisulfite conversion using an EZ DNA Methylation-Gold Kit (catalog number D5005; Zymo Research Corp., Irvine, CA, USA) and PCR amplification, the high-quality libraries were sequenced on an Illumina sequencing platform in PE150 mode. The clean reads were mapped to the reference genome (SL3.0) with BSSEEKER software (Guo *et al.*, 2013). CGMAP Tools (Guo *et al.*, 2018) was used to analyze the sequencing depth of C bases across the genome, the differentially methylated regions (DMRs), and the methylation level distribution in the gene body region and the regions 2 kb upstream and downstream of the gene body for all samples. The methylation level was determined by dividing the number of reads covering each methylcytosine by the total number of reads covering that cytosine, which was also equal to the methylcytosine/cytosine ratio at each reference cytosine. The CIRCLIZE package (Gu *et al.*, 2014) was used to plot the distributions of methylated C sites, DMRs and copy number variations in the genome.

### McrBC-PCR and McrBC-qPCR analysis

Genomic DNA were extracted and purified from fruit pericarp using the illustra DNA extraction kit Phytopure (Tiangen, Beijing, China). 1 µg of genomic DNA was digested with McrBC (New England Biolabs, Beverly, MA, USA), a methylation-dependent restriction enzyme that cuts methylated but not unmethylated DNA, for 5 h according to manufacturer instructions with or without guanosine triphosphate. McrBC-PCR and McrBC-qPCR were performed with 50 and 20 ng DNA, respectively. The primers used for McrBC-PCR and McrBC-qPCR analysis are listed in Dataset S1.

### Analysis of publicly available WGBS data

Whole-genome bisulfite sequencing data from *dml2* and WT tomato (GSE94903) (Lang *et al.*, 2017) were analyzed.

### Statistical analysis

Data are expressed as means ± SE. Differences among treatments were determined by ANOVA, followed by Student's *t*-test. Statistical analysis was performed using SPSS v.7.5 (SPSS Inc., Chicago, IL, USA).

## Results

### SIJMJ7 is a repressor of fruit ripening

Among histone demethylases, JMJs have more diverse specificities, sequences and functions than LSD1 family proteins, which have been classified into several subgroups, including the KDM5/JARIDA1 subgroup (Mosammaparast & Shi, 2010). The KDM5 subgroup is probably one of the most widely studied JMJs. Based on the sequences of Arabidopsis homologs, we identified four KDM5/JARIDA1-type JMJs in tomato, named SIJMJ5 (Soly04g009990.2.1), SIJMJ6 (Soly06g008490.2.1), SIJMJ7 (Soly02g069740.2.1) and SIJMJ8 (Soly08g081000.2.1). Phylogenetic analysis revealed that SIJMJ5, SIJMJ6, SIJMJ7 and SIJMJ8 have high similarity to AtJMJ16, AtJMJ19, AtJMJ14 and AtJMJ17 in Arabidopsis, respectively (Fig. S1). AtJMJ14 plays a versatile role in regulating plant biological processes, including flowering time (Lu *et al.*, 2010), circadian rhythm (Song *et al.*, 2019), RNA silencing (Le Masson *et al.*, 2012), RNA-directed DNA methylation (Deleris *et al.*, 2010) and immune response (D. Li *et al.*, 2020). AtJMJ16 is a negative important regulator of leaf senescence through demethylating H3K4 at senescence-associated genes (Liu *et al.*, 2019), whereas AtJMJ17 regulates ABA-responsive genes (Wang *et al.*, 2021) and dehydration stress response (H. Huang *et al.*, 2019; S. Huang *et al.*, 2019). Our previous study showed that the expression of *SIJMJ7* is more enormously upregulated during tomato fruit ripening, compared with other KDM5/JARIDA1 members, implying that SIJMJ7 might be implicated in the regulation of fruit ripening in tomato. Therefore, we focused specifically on characterizing the function and mechanism of action of SIJMJ7 in fruit ripening.

We first generated 37 *SIJMJ7* overexpression lines, from which we selected two independent lines, *SIJMJ7-OE7* and *SIJMJ7-OE9*, because of their significantly high expression levels of the *SIJMJ7* transcript (Fig. 1a) and the SIJMJ7 protein (Fig. 1b). We also used the CRISPR-Cas9 gene editing system to construct stable loss-of-function *SIJMJ7* mutants in which an sgRNA specifically targeted the first exon of *SIJMJ7* (Fig. S2a), and selected two independent lines with truncated proteins, *sljnj7-1* and *sljnj7-2* (with deletions of 203 and 61 bp, respectively, in the first exon of *SIJMJ7*) (Fig. S2b). Neither the *SIJMJ7* transcript (Fig. 1c) nor the SIJMJ7 protein (Fig. 1d) was detected in these two mutant lines. Examination of these transgenic lines revealed that the *SIJMJ7-OE* lines displayed a late fruit ripening phenotype (average 3.5 d late), whereas loss of function of *SIJMJ7* accelerated fruit ripening (average 4.7 d earlier) (Fig. 1e). Furthermore, *SIJMJ7-OE* fruits had lower ethylene production rates and α-carotene and lycopene concentrations, but higher Chl content, than WT fruits at 38 and 42 dpa (Fig. 1f). In contrast to the *SIJMJ7-OE* lines, *sljnj7* mutants exhibited the opposite patterns for all of these physiological traits, except for lycopene content at 42 dpa (Fig. 1f). These data suggest that SIJMJ7 functions as a repressor of tomato fruit ripening. In addition, we also found that *sljnj7* mutants exhibited an early flowering phenotype (no shown data). Therefore, in addition to its involvement in

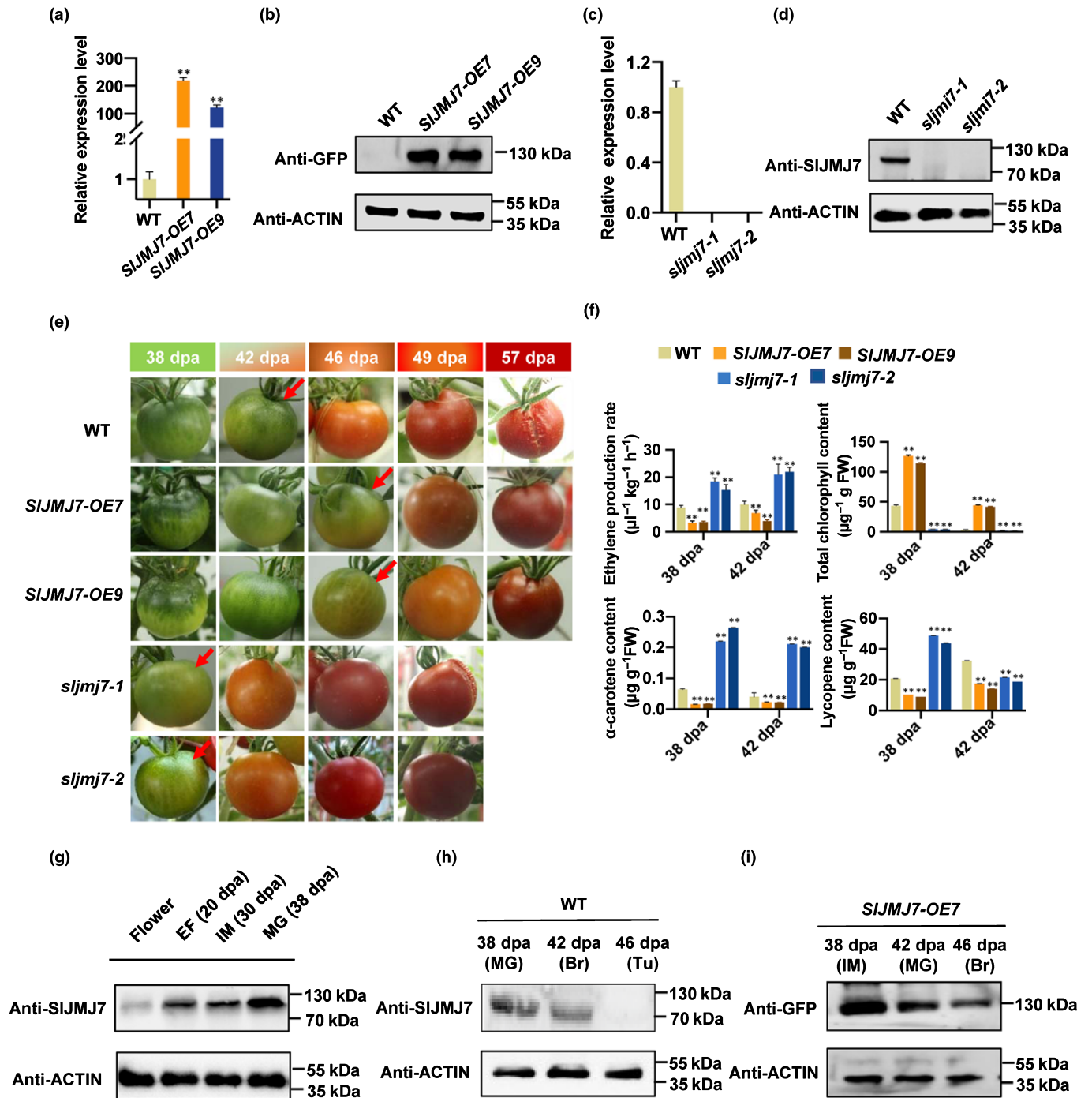


**Fig. 1** *SLMJ7* is a repressor of fruit ripening in tomato. (a) Analysis of the gene expression level of *SLMJ7* in the *SLMJ7-OE7* and *SLMJ7-OE9* lines by real-time quantitative polymerase chain reaction (RT-qPCR). Gene expression in the wild-type (WT) was set as 1. *ACTIN* was used as the internal control. The data are presented as the means  $\pm$  SE of three replicates. The significant differences from the WT are indicated by asterisks (Student's *t*-test; \*\*,  $P < 0.01$ ). (b) Western blot analysis of the protein abundance of *SLMJ7* in the *SLMJ7-OE7* and *SLMJ7-OE9* plants. An anti-GFP antibody was used for detection, and an anti-ACTIN antibody was used for internal control analysis. (c) Measurement of the *SLMJ7* gene expression levels in the *sljmj7-1* and *sljmj7-2* lines by RT-qPCR. Gene expression in the WT was set as 1. *ACTIN* was used as the internal control. (d) Western blot analysis of the protein abundance of *SLMJ7* in the *sljmj7-1* and *sljmj7-2* lines. An anti-*SLMJ7* antibody was used for detection, and an anti-ACTIN antibody was used for internal control analysis. (e) Fruit phenotypes of the WT line, the *SLMJ7* overexpression lines *SLMJ7-OE7* and *SLMJ7-OE9*, and the *sljmj7* knockout mutants *sljmj7-1* and *sljmj7-2* during the fruit-ripening process. The red arrows indicate the color break from the WT lines, the *SLMJ7-OE7* and *SLMJ7-OE9* lines, and the *sljmj7-1* and *sljmj7-2* lines. (f) Ethylene production rate (upper left), contents of total chlorophyll (upper right),  $\alpha$ -carotene (lower left) and lycopene (lower right) in the fruits of the WT, *SLMJ7-OE* lines and *sljmj7* mutants at 42 and 46 d post-anthesis (dpa). The data are presented as the mean  $\pm$  SE of three replicates. The significant differences from the WT are indicated by asterisks (Student's *t*-test; \*\*,  $P < 0.01$ ). (g) Protein abundance of *SLMJ7* in tomato flowers and fruits at various developmental stages. EF, early fruit; IM, immature; MG, mature green. (h) The protein abundance of *SLMJ7* in WT fruits at the MG, color break (Br) and turning (Tu) stages. (i) Protein abundance of *SLMJ7* in *SLMJ7-OE7* fruits at the MG, Br and Tu stages.

regulating fruit ripening, SIJMJ7 might be implicated in flowering regulation like its homolog AtJMJ14 in Arabidopsis.

We next examined SIJMJ7 protein expression profiles in WT fruits at different ripening stages using Western blot with an anti-SIJMJ7 antibody. SIJMJ7 expression increased from the early fruit (EF; 20 dpa) to the immature (IM; 30 dpa) to the mature green (MG; 38 dpa) stages (Fig. 1g). However, the protein abundance of SIJMJ7 markedly decreased in WT fruits from the MG to the color break (Br; 42 dpa) to the turning stage (Tu; 46 dpa) (Fig. 1h). Consistent with this pattern, a decrease in the SIJMJ7 protein abundance was also detected in *SIJMJ7-OE7* fruits from the IM to the Br to the Tu stage (Fig. 1i). These data demonstrate that the SIJMJ7 protein accumulates at the onset of tomato fruit ripening but decreases at the Br stage. Together, these results indicated that SIJMJ7 plays a role in regulating tomato fruit ripening as a repressor.

### SIJMJ7 is a site-specific histone H3K4 demethylase

As SIJMJ7 contains a JmjC domain, which has a histone demethylation function, we investigated whether SIJMJ7 exerts a specific type of histone demethylase activity *in vivo*. GFP-fused SIJMJ7 was transiently expressed in the epidermal cells of tobacco leaves, and the signal intensities of various histone lysine methylation marks were detected by immunofluorescence. SIJMJ7-GFP was localized in the nucleus, and SIJMJ7-GFP expression markedly decreased the signal intensities of mono-, di-, and trimethylated H3K4 in the nucleus, with the greatest effect for H3K4me3 (Fig. 2a). However, the methylation signals at the H3K9, H3K27 and H3K36 sites showed no obvious changes (Figs S3–S5). Moreover, the H3K4 demethylase activity of SIJMJ7-GFP was abolished when His288 and Glu290, the two conserved iron-binding amino acids (Fig. S6), were replaced with alanines (Fig. 2b), suggesting that these amino acids are crucial for the histone H3K4 demethylase activity of SIJMJ7. The H3K4 demethylase activity was further confirmed when we compared the histone methylation profiles of WT, *sljmj7 mutant* and *SIJMJ7-OE* plants by Western blot. The degrees of mono-, di-, and trimethylation at H3K4 but not H3K9, H3K27 and H3K36 were higher in *sljmj7 mutant* (Fig. 2c,d) and lower in *SIJMJ7-OE* plants (Fig. 2e,f) than those in WT plants. To confirm the *in vitro* enzymatic activity of SIJMJ7, we transiently expressed SIJMJ7-GFP in tobacco leaf cells, and SIJMJ7-GFP was immunoaffinity-purified. As shown in Fig. 2 (g,h), the SIJMJ7-GFP decreased the levels of H3K4me3, H3K4me2 and H3K4me1, rather than H3K9me1/2/3, H3K27me1/2/3 and H3K36me1/2/3. Collectively, these data reveal that SIJMJ7 is a histone H3K4 site-specific demethylase in tomato.

### SIJMJ7 represses target gene expression by demethylating H3K4me3

Because SIJMJ7 is an H3K4me3 demethylase (Fig. 2) and H3K4me3 is usually associated with gene activation, we hypothesized that SIJMJ7 might negatively regulate the expression of ripening-related genes. To examine the role of SIJMJ7 in

regulating fruit ripening, we analyzed the SIJMJ7-regulated transcriptome by deep RNA sequencing (RNA-seq) of WT and *sljmj7-1* fruits at 38 dpa. *sljmj7-1* was randomly selected for the remainder of study because *sljmj7-1* fruits exhibited an early fruit ripening phenotype. At 38 dpa, the WT fruits were at the MG stage, whereas the *sljmj7-1* fruits were at the break stage. Compared with WT fruits, in *sljmj7-1* fruits 3087 genes were upregulated and 2092 genes were downregulated (Datasets S2, S3). The functional categories of the upregulated genes in the *sljmj7-1* mutant were mainly related to photosynthesis, sugar metabolism, mitogen-activated protein kinase (MAPK) signaling, starch and sucrose metabolism and plant hormone signal transduction (Fig. 3a). By contrast, the downregulated gene categories in the *sljmj7-1* fruits were mainly related to amino acid biosynthesis, cysteine and methionine metabolism, and peroxisome and terpenoid-quinone biosynthesis (Fig. 3a). RNA-seq analysis revealed that a number of genes corresponding to ripening-associated processes, such as ethylene biosynthesis, transcriptional regulation, carotenoid biosynthesis, flavonoid/anthocyanin biosynthesis and cell wall organization, were upregulated in the *sljmj7-1* mutant (Fig. 3b). The reliability of RNA-seq data was further confirmed by RT-qPCR. The expression of nine fruit ripening-related genes, including *E8*, *NR*, *CHS1*, *PSY1*, *ZISO*, *LoxC*, *XYL1*, *PL1* and *PG2a*, were verified to be upregulated in the *sljmj7-1* fruits, and downregulated in the *SIJMJ7-OE7* fruits, except for *XYL1* and *PG2a*, compared with WT fruits (Fig. S7). Taken together, these data indicate that SIJMJ7 may suppress fruit ripening by regulating the transcription of the genes involved in the ripening-related processes, including ethylene biosynthesis, transcriptional regulation, carotenoid biosynthesis, flavonoid/anthocyanin biosynthesis and cell wall organization.

To identify the direct targets of SIJMJ7 on a genome-wide scale, we performed ChIP-seq analysis with an anti-GFP antibody in the *SIJMJ7-OE7* (with GFP tag) fruits at 38 dpa (MG stage). A total of 8118 common peaks from three biological replicates were identified and considered to correspond to the direct binding sites of SIJMJ7 (Dataset S4). These binding sites were randomly distributed on different chromosomes in tomato (Fig. S8). Most of the SIJMJ7 binding sites (61.33%) were located in gene body regions, while 19.11% and 19.56% of the sites were located in intergenic and promoter regions, respectively (Fig. 3c). Read density analysis further showed that these SIJMJ7 binding sites were uniformly distributed between the transcription start site (TSS) and the transcription end site (TES) (Fig. 3d). Motif enrichment analysis demonstrated that SIJMJ7 bound to motifs of its potential targets such as *Bapx1* (24.64%), *LRF* (22.02%), *TCX2* (18.40%), *SOL1* (18.02%) and *NFI* (13.78%) (Fig. 3e). It is suggested that SIJMJ7 may be recruited to its targets by sequence-specific transcription factors.

Trimethylation of H3K4 is a global epigenetic mark that is usually associated with gene activation (Klose & Zhang, 2007). As SIJMJ7 has H3K4 demethylase activity, we further examined whether SIJMJ7 regulates the expression of target genes by removing H3K4me3. Genome-wide H3K4me3 profiles were analyzed by ChIP-seq with an anti-H3K4me3 antibody in WT

and *slmj7-1* fruits at 38 dpa. A total of 1375 sites were identified to have increased levels of H3K4me3 (fold change > 2) and 779 sites displayed decreases in H3K4me3 in the *slmj7* mutant relative to the WT (Dataset S5). These sites exhibiting SIJM7-mediated H3K4me3 demethylation were distributed across

different gene regions, including the promoter-TSS, TTS, exons, introns and intergenic regions, of which exons (33.11%) and introns (24.98%) accounted for the largest proportions across the genome (Fig. 3f). In addition, the distribution of H3K4me3 and heat map analysis in the WT and *slmj7-1* mutant showed that

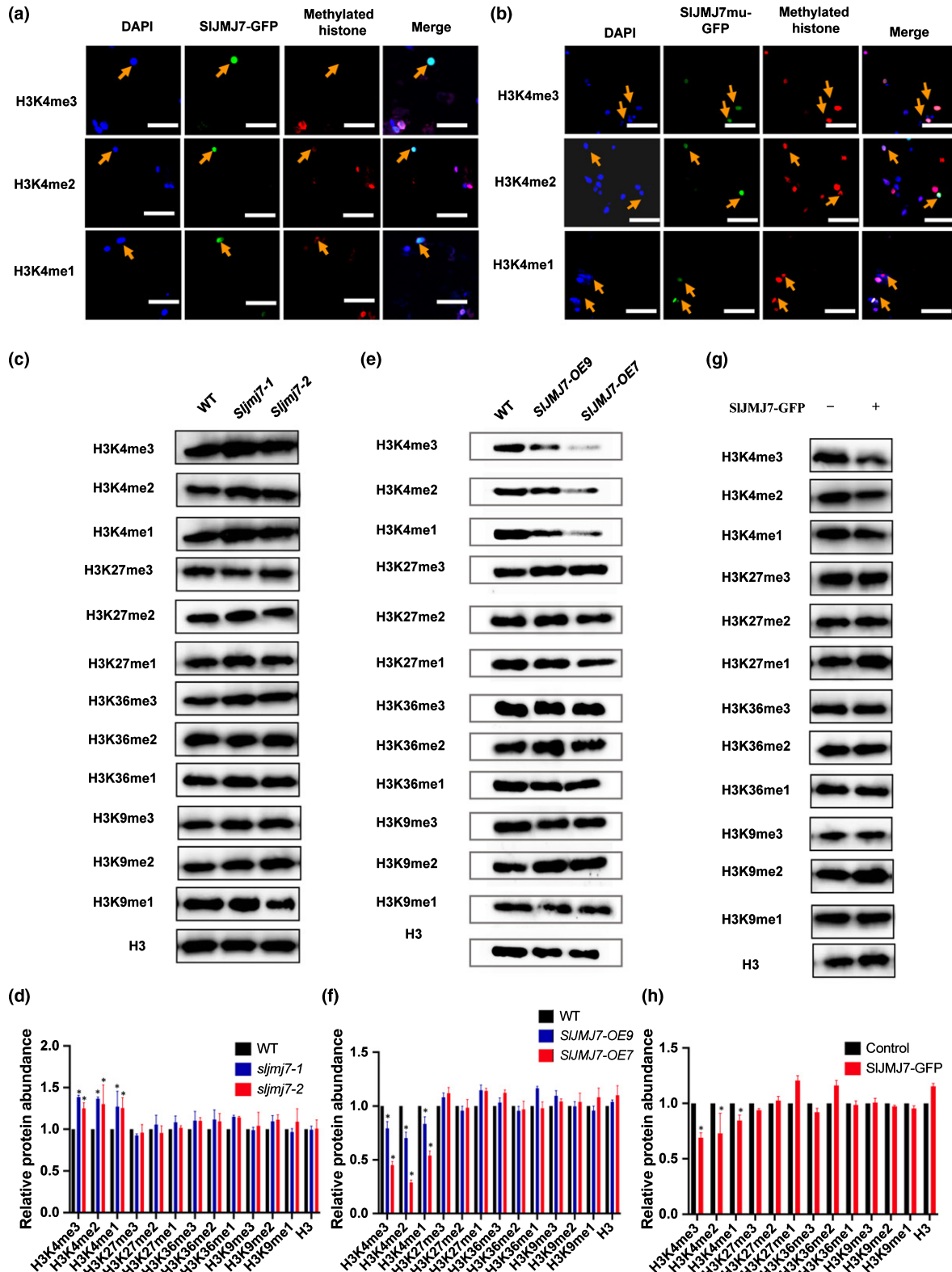


**Fig. 2** *SIJMJ7* is a histone H3K4 demethylase in tomato. (a, b) Analysis of the histone demethylase activity of *SIJMJ7* in tobacco leaves by an immunofluorescence assay. Nuclei transfected with *SIJMJ7*-GFP (a) or *SIJMJ7*<sup>H288A/E290A</sup>-GFP mutants (two conserved iron-binding amino acids mutation) (b). Nuclei were stained with 4',6-diamidino-2-phenylindole staining (DAPI, blue, left). *SIJMJ7*-GFP and *SIJMJ7m*-GFP expression in *Nicotiana benthamiana* nuclei was visualized by monitoring GFP fluorescence (green, middle). The histone methylation status was analyzed by immunostaining with specific histone methylation antibodies (red, right). Bars, 50 µm. Orange arrows indicate nuclei transfected with *SIJMJ7*-GFP. (c) Detection of changes in histone methylation levels in the wild-type (WT) and *sljmj7-1* and *sljmj7-2* lines by Western blot. (d) Statistical analysis of (c). (e) Detection of changes in histone methylation levels in the WT, *SIJMJ7-OE7* and *SIJMJ7-OE9* lines by Western blot. (f) Statistical analysis of (e). (g) *In vitro* demethylase activity of *SIJMJ7*. Calf histone was incubated with (+) or without (-) tobacco cell-expressed *SIJMJ7*-GFP fusion protein and analyzed by Western blot using specific antibodies indicated on the left. (h) Statistical analysis of (g). Antibodies against mono-, di-, and trimethylated K4, K9, K27 and K36 of histone H3 were used to detect the presence of each modification. In (d, f, h), the immunoblot signals relative to the WT (set as 1) were quantified. The data are presented as means ± SE of three replicates (Student's *t*-test; \*, *P* < 0.05).

H3K4me3 sites were located mainly in promoter regions and 5'-end regions of the gene body (Fig. 3g,h). In the *sljmj7* fruit, the elevated H3K4me3 levels might facilitate the expression of its target genes.

As H3K4me3 is found at the TSS of many expressed genes, therefore mutation of a H3K4me3 demethylase will inevitably impact gene expression. To discern the direct *SIJMJ7*-regulated genes, we combined the results from RNA-seq and two ChIP-seq datasets (with the anti-GFP antibody and the anti-H3K4me3 antibody). These genes bound by *SIJMJ7* with upregulated expression and increased H3K4me3 levels in *sljmj7* compared with the WT were defined as direct targets of *SIJMJ7*, and the other genes were considered to be indirectly regulated by *SIJMJ7*. As a result, a Venn diagram showed that 262 genes were directly regulated by *SIJMJ7*-mediated H3K4me3 demethylation (Fig. 3i; Dataset S6). These genes relate mainly to cysteine and methionine metabolism; valine, leucine and isoleucine biosynthesis; MAPK signaling pathway; and indole alkaloid biosynthesis (Fig. 3j). Additionally, a number of genes related to ethylene biosynthesis (*ACS2*, *ACS4*, *ACS8* and *ACO6*), transcription regulation (*RIN*, *NOR* and *CNR*), carotenoid biosynthesis (*PSY1*, *PDS*, *PTOX*, *CHY2*, *ZISO*, *GGPPS2* and *CHS1*), cell wall modification (*CEL2*, *XTH5*, *EXP1*, *XYL1*, *PG2a*, *TBG4*, *PL1*, *PL2* and *PL8*), and flavonoid/anthocyanin biosynthesis (*4CL*, *LoxB*, *LoxC* and *BCAT1*) were directly repressed by *SIJMJ7*-mediated H3K4me3 demethylation (Dataset S6). These data suggest that *SIJMJ7* represses the expression of target genes, especially those associated with fruit ripening regulation, by removing H3K4me3.

### *SIJMJ7* binds to key ripening-related genes and represses their expression via H3K4me3 demethylation

As several ripening-related genes were found to be directly repressed by *SIJMJ7*-mediated H3K4me3 demethylation, we further confirmed the binding and H3K4me3 modification of ethylene biosynthesis genes (*ACS2* and *ACS4*) and transcription regulators (*RIN* and *NOR*) by *SIJMJ7* using ChIP-qPCR. The integrated genome browser visualization clearly showed that *SIJMJ7* was enriched in the gene body regions of the ripening-related genes (Fig. 4a). Furthermore, the *SIJMJ7* binding sites and H3K4me3 modification sites overlapped well on the ripening-related genes (Fig. 4a,b). Two different loci (*P1* and *P2*) were selected to analyze the binding of *SIJMJ7* with the loci of *ACS2*, *ACS4*, *RIN* and *NOR* genes. ChIP-qPCR verified that *SIJMJ7* directly bound to these genes during fruit ripening (Fig.

4c). We also analyzed H3K4me3 methylation status at the *ACS2*, *ACS4*, *RIN* and *NOR* loci by amplifying two different loci (*P1* and *P2*). The H3K4me3 levels of these genes were significantly higher in the *sljmj7-1* mutant than in the WT (Fig. 4d). Additionally, the loci of the genes related to flavonoid/anthocyanin biosynthesis (*CHS1* and *LoxC*) and carotenoid biosynthesis (*PSY1* and *ZISO*) were bound by *SIJMJ7* and had significantly higher H3K4me3 methylation levels in the *sljmj7-1* fruits than in the WT fruits (Figs S9–S11). RT-qPCR further confirmed that the expression of the key ripening-related genes, including *ACS2*, *ACS4*, *RIN*, *NOR*, *CHS1*, *LoxC*, *PSY1* and *ZISO*, were significantly upregulated in the *sljmj7-1* fruits and downregulated in the *SIJMJ7-OE7* fruits compared with the WT fruits (Figs 4e, S7). To further elucidate the role of *SIJMJ7*-mediated demethylation of H3K4me3 in fruit ripening, we analyzed the binding activity of *SIJMJ7* at the binding regions and H3K4me3 level changes on the chromatin of *ACS2*, *ACS4*, *RIN* and *NOR*, as well as the expression of these genes in the WT during the ripening process. Consistently, the binding of *SIJMJ7* at the binding regions on the chromatin of *ACS2*, *ACS4*, *RIN* and *NOR* increased from EF to the MG stage and decreased as ripening progressed (Br stage) (Fig. 4f); however, the H3K4me3 level (Fig. 4g) and the transcription level (Fig. 4h) of these genes showed the opposite trends. Therefore, these findings demonstrate that *SIJMJ7* directly represses the expression of a number of key ripening-related genes by H3K4me3 demethylation during tomato fruit ripening.

### *SIJMJ7*-mediated removal of H3K4me3 represses the expression of *DML2* during fruit ripening

Strikingly, combined genome-wide transcription, binding sites and histone modification profile analyses identified *DML2*, a key DNA demethylase gene, as a direct target of *SIJMJ7* (Dataset S6), implying that *SIJMJ7* possibly indirectly regulates DNA methylation via *DML2*. To confirm the speculation, we investigated the dynamic regulation of *DML2* by *SIJMJ7*. The genome browser visualization showed that *SIJMJ7* binding occurred in the gene body region of *DML2* (Fig. 5a). Given that *SIJMJ7* was highly expressed from EF to MG stages but decreased as ripening progressed (Br stage) (Fig. 1g–i), we next analyzed the dynamic binding of *SIJMJ7* at the *DML2* locus during fruit ripening. ChIP-qPCR analysis showed that *SIJMJ7* was highly enriched at the *DML2* locus in the WT fruits at 38 dpa (MG stage), whereas the *SIJMJ7* binding level significantly decreased at 42 dpa (Br stage)

(Fig. 5b). To validate this result, we analyzed the dynamic binding of SIJMJ7 at the *DML2* locus in the *SIJMJ7-OE* fruits at 42 dpa (MG stage) and 46 dpa (Br stage). Consistent with the results described earlier, SIJMJ7 was highly enriched at the *DML2* locus

at the MG stage, but its binding was significantly decreased at the Br stage in the *SIJMJ7-OE* fruits (Fig. 5c). These results suggest that the binding of SIJMJ7 at the *DML2* gene locus decreases during early fruit ripening.

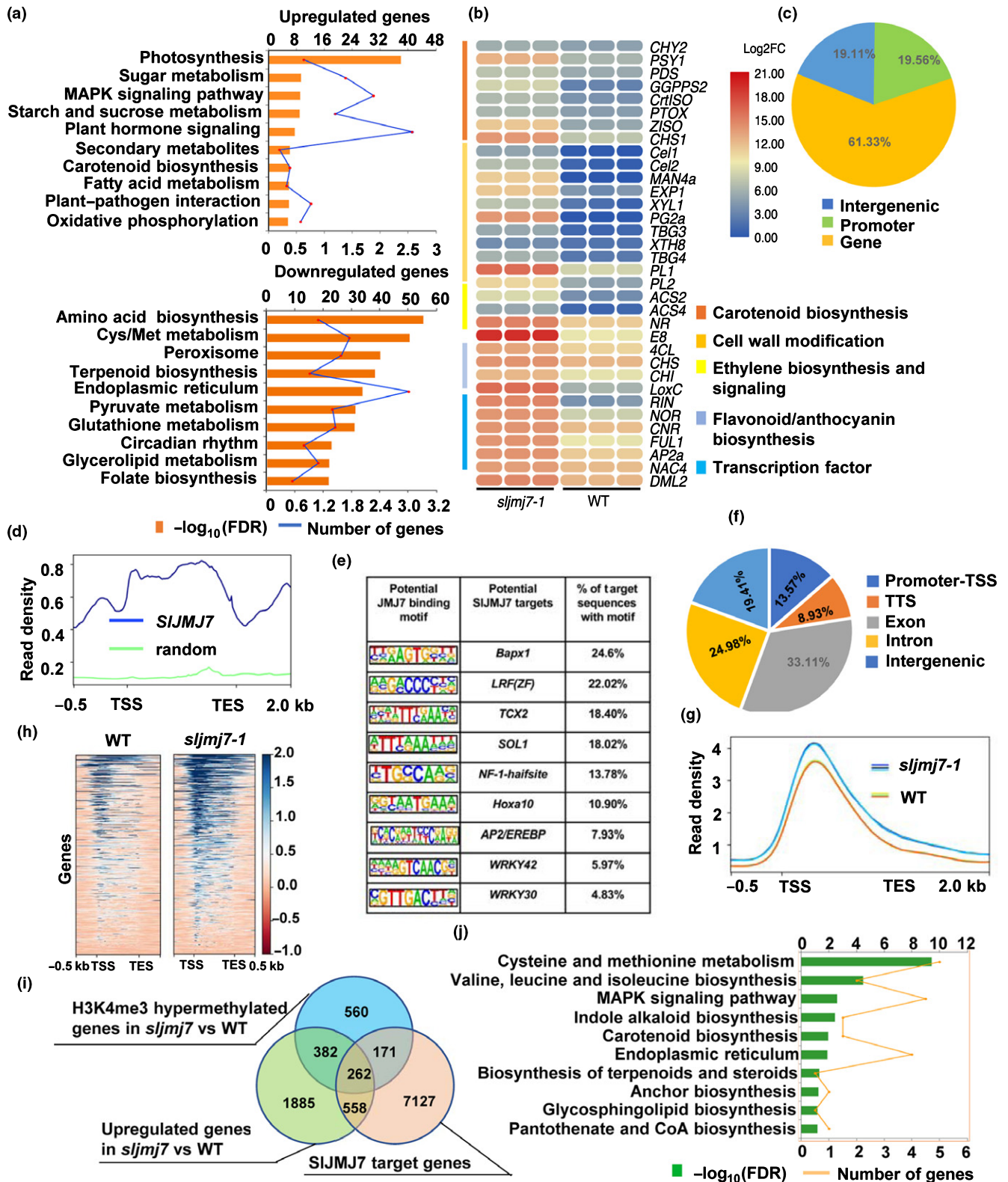


**Fig. 3** *SIJMJ7* represses target gene expression by demethylating H3K4me3 in tomato. (a) RNA-seq analysis of the *SIJMJ7*-regulated transcriptome during fruit ripening. DAVID functional clustering analysis of the gene clusters in the *sljmj7-1* mutant that were upregulated (upper) and downregulated (lower) compared with those in the wild-type (WT). Transcription levels of the representative ripening-related genes in the WT and *sljmj7-1* mutant. (b) These genes were group into five classes as indicated. (c) Distribution of *SIJMJ7* binding sites in different regions of annotated genes. (d) Normalized read density of *SIJMJ7*-GFP chromatin immunoprecipitation sequencing (ChIP-seq) signals in the gene bodies of *SIJMJ7* target genes and the same number of randomly selected genes. (e) Binding motifs in *SIJMJ7*-targeted regions. The 10 most abundant motifs are listed. The size of the letter for each nucleotide represents the conservation. (f) Distribution of sites with *SIJMJ7*-mediated H3K4me3 demethylation in different regions of annotated genes of the *sljmj7-1* mutant. (g) The intensities of H3K4me3 in the WT and *sljmj7-1* mutant fruits. The region shown is from 0.5 kb upstream to 2 kb downstream of the transcription start site (TSS). (h) Heat maps of the gene body regions of *SIJMJ7* target genes ranked by H3K4me3 levels in the WT and *sljmj7-1* fruits. (i) Venn diagram of the overlapping *SIJMJ7*-targeted, *SIJMJ7*-repressed and H3K4me3-demethylated genes. (j) DAVID functional clustering analysis of the gene clusters with binding of *SIJMJ7* and repression via *SIJMJ7*-mediated H3K4me3 demethylation.

As previous work reported that induction of *DML2* expression occurs after the Br stage (Liu *et al.*, 2015), we next examined the dynamic expression profile of *DML2* in WT and *sljmj7-1* fruits during fruit ripening. Consistent with the previous findings (Liu *et al.*, 2015), a burst of *DML2* expression was detected at 42 dpa (Br stage) in the WT fruits (Fig. 5d). Furthermore, *DML2* expression in the *sljmj7* mutant fruits were significantly upregulated compared with those in the WT fruits at 38 and 42 dpa (Fig. 5d). Therefore, *SIJMJ7* may specifically repress *DML2* gene expression during fruit ripening.

Finally, we evaluated the dynamic change in the H3K4me3 level at the *DML2* locus in WT and *sljmj7-1* fruits. The genome browser visualization showed that mutation of *SIJMJ7* in tomato (*sljmj7-1*) led to a significant increase in the H3K4me3 level at the *DML2* locus (Fig. 5e). Consistent with the expression pattern of *DML2*, the P1 and P2 regions of *DML2* had higher levels of H3K4me3 at 42 dpa than at 38 dpa in the WT fruits (Fig. 5f). Moreover, the H3K4me3 levels at the P1 and P2 regions of the *DML2* locus in the *sljmj7-1* mutant fruits were significantly elevated compared with those in the WT fruits at both stages. Notably, the fold changes between *sljmj7-1* and WT fruits were markedly higher at 38 dpa than at 42 dpa for both regions (Fig. 5f). Collectively, these data suggest that *SIJMJ7* directly and specifically represses *DML2* expression via H3K4me3 demethylation during fruit ripening.

### The link between histone demethylation and DNA demethylation

The direct repression of *DML2* expression by *SIJMJ7* prompted us to investigate whether loss of function of *SIJMJ7* affects the DNA methylome during fruit ripening. Wild-type and *sljmj7-1* fruits at 38 dpa were subjected to WGBS analysis with three biological replicates per line to determine the methylome. Differentially methylated regions in three contexts – CG, CHG, and CHH (where H denotes A, T, or C) – were determined by comparing the methylation levels in *sljmj7* mutant fruits with those in WT fruits. Over 91.9% of the genomic cytosines were covered in each sample, and each methylome was sequenced with a coverage of at least 18-fold per DNA strand (Dataset S7). Compared with the WT fruits, in the *sljmj7* fruits 11 585, 5081, and 203 DMRs in the CG, CHG, and CHH contexts, respectively, were hypomethylated (hypo-DMRs) (Fig. 6a; Datasets S8–S10). By contrast, only 249, 978 and 74 DMRs in the CG, CHG and

CHH contexts, respectively, were hypermethylated (hyper-DMRs) in the *sljmj7* mutant fruits compared with the WT fruits (Datasets S11–S13). The overwhelmingly higher numbers of hypo-DMRs than hyper-DMRs in the *sljmj7* fruits than in the WT fruits were consistent with activated *DML2* expression, and reveal that *sljmj7* mutation can cause global DNA hypomethylation in tomato fruits.

Previous work determined the DNA methylation profile of *dml2* mutants and identified a larger number of hyper-DMRs than hypo-DMRs in these mutants (Lang *et al.*, 2017). In order to explore the genes jointly regulated by *SIJMJ7* and *DML2* in relation to DNA demethylation, we conducted a combined analysis of two methylome data, hypo-DMRs in *sljmj7* vs WT and hyper-DMRs *dml2* vs WT. The hyper-DMRs in *dml2* vs WT were derived from published data (Lang *et al.*, 2017). Like *DML2* targets (16), hypo-DMRs also aggregated in chromosomal arms in the *sljmj7* mutant (Fig. 6b). Furthermore, broadly in accordance with the fact that *DML2* preferentially targets the intergenic (IG) and transposable element (TE) regions in tomato (Lang *et al.*, 2017), we showed that the hypo-DMRs in the *sljmj7* mutant were located mostly in the TE (25.72%), promoter (24.12%), IG (15.45%) and exon (14.69%) regions (Fig. 6c), whereas the hyper-DMRs were enriched in the TE (44.66%), intron (29.59%), and IG (13.88) regions (Fig. S12). We further analyzed the overlapping hypo-DMRs in the *sljmj7* mutant and hyper-DMRs in the *dml2* mutant in three contexts – CG, CHG and CHH – and found that the hypo-DMRs in *sljmj7* and the hyper-DMRs in *dml2* overlapped well; 40.27% (2493 of 6191) of the hypo-DMRs in the *sljmj7* mutant were hypermethylated in the *dml2* mutant (Fig. 6d; Dataset S14), indicating that *SIJMJ7* regulates DNA methylation via *DML2*.

Interestingly, the *SIJMJ7*-bound key ripening-related transcription factors *RIN* and *NOR* were hypomethylated in the *sljmj7* mutant compared with the WT (Fig. 6e,f). This result was further confirmed by McrBC-PCR and McrBC-qPCR (Fig. 6g,h). Moreover, the hypo-DMRs in the *sljmj7* mutant were found in a relatively large number of genes related to ripening processes, including ethylene biosynthesis (*ACS2*, *ACS4*, *ACS8*, *ACO6*), transcription regulation (*RIN*, *NOR*), carotenoid metabolism (*PSY1*, *ZISO*) and cell wall degradation (*EXP1*, *XYL1*, *TBG4*, *PL1*, *PL2*, *PL8*) (Datasets S15–S17; Fig. S13). As these genes have been reported to be direct targets of *DML2* (Lang *et al.*, 2017), these results suggest that *SIJMJ7* may indirectly repress their expression via *DML2*-mediated DNA demethylation in tomato fruit.

Taken together, these findings demonstrate that *SIJMJ7* may regulate the DNA methylome by repressing *DML2* expression during fruit ripening. Moreover, *SIJMJ7* may regulate the expression of ripening-related genes via *DML2*-mediated DNA demethylation.

## Discussion

Histone methylation modification plays essential roles in multiple developmental processes in plants, including flowering, shoot development, stem elongation and leaf senescence

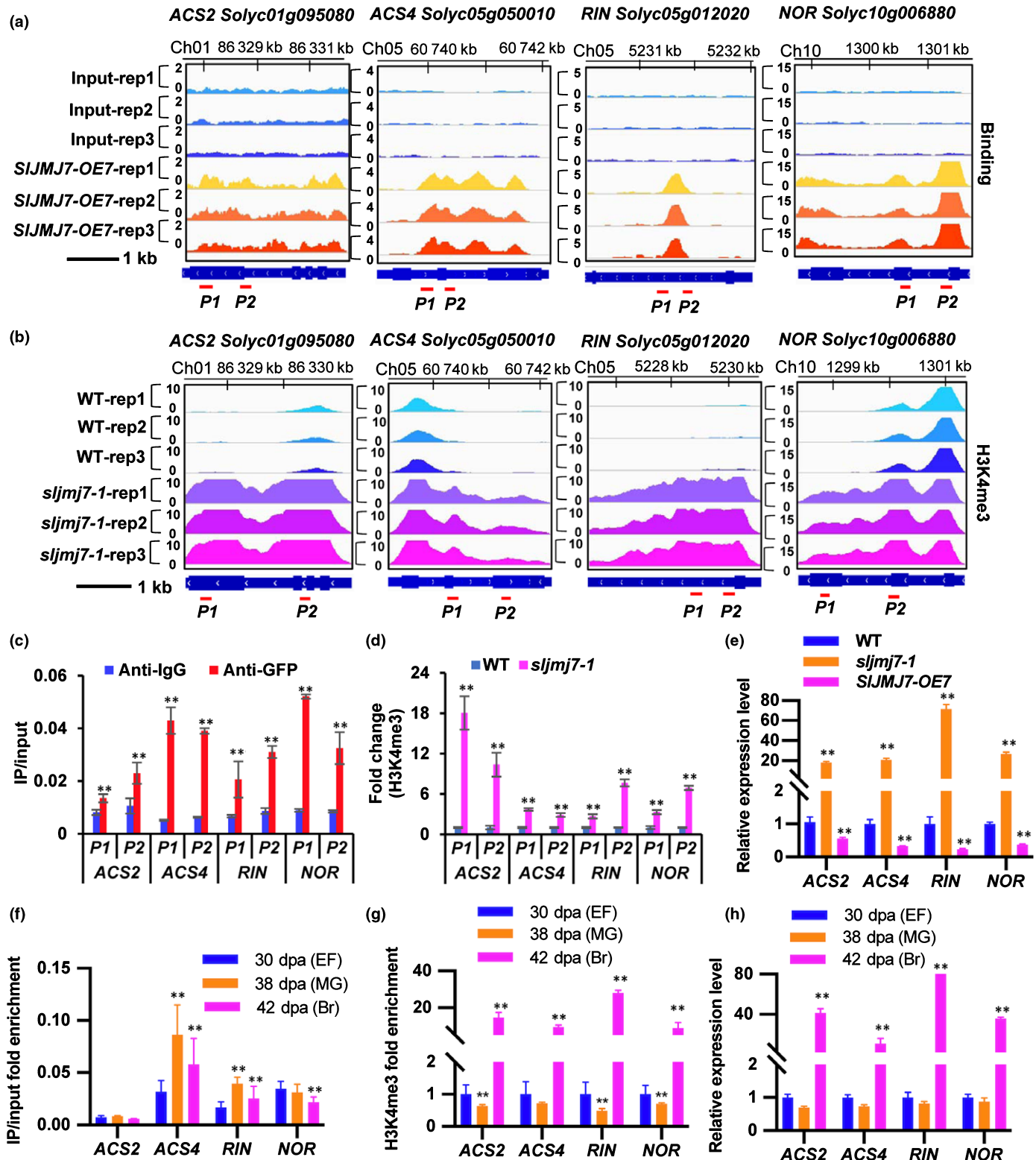


**Fig. 4** *SIJMJ7* binds directly to key ripening-related genes and represses their expression by removing H3K4me3 in tomato. (a) Genome browser visualization of the binding sites of the key ripening-related genes *ACS2*, *ACS4*, *RIN* and *NOR* detected by chromatin immunoprecipitation sequencing (ChIP-seq) in the *SIJMJ7-OE* fruits. (b) Genome browser visualization of the H3K4me3 levels of the *ACS2*, *ACS4*, *RIN* and *NOR* genes in the WT and *sljmj7-1* fruits. (c) Verification of *SIJMJ7* binding to *ACS2*, *ACS4*, *RIN* and *NOR* genes by ChIP-quantitative PCR (ChIP-qPCR). Fruits of *SIJMJ7-OE7* plants at 38 d post-anthesis (dpa) were used for analysis. An anti-GFP antibody was used for immunoprecipitation, and immunoglobulin G (IgG) was used as the negative control. (d) ChIP-qPCR analysis of the H3K4me3 levels of ripening-related genes in the WT and *sljmj7-1* mutant. An anti-H3K4me3 antibody was used for immunoprecipitation. *ACTIN* was used as the internal control. (e) Real-time quantitative polymerase chain reaction (RT-qPCR) analysis of *ACS2*, *ACS4*, *RIN* and *NOR* expression levels in the WT, *sljmj7-1* and *SIJMJ7-OE7* fruits at 38 dpa. *ACTIN* was used as the internal control. (f) The binding of *SIJMJ7* at the binding regions on the chromatin of *ACS2*, *ACS4*, *RIN* and *NOR* in WT fruit at 30, 38 and 42 dpa. (g) H3K4me3 levels on the chromatin of *ACS2*, *ACS4*, *RIN* and *NOR* in WT fruit at 30, 38 and 42 dpa. (h) Expression of *ACS2*, *ACS4*, *RIN* and *NOR* in WT fruit at 30, 38 and 42 dpa. In (a, b), gene structures of *ACS2*, *ACS4*, *RIN* and *NOR* are shown underneath. In (a), *P1* and *P2* indicate the amplified regions by ChIP-qPCR in (c). In (b), *P1* and *P2* indicate the amplified regions by ChIP-qPCR in (d). Bar, 1 kb. Three biological replicates were used for the fruits of the WT, *SIJMJ7-OE* lines and *sljmj7* mutants. The data are presented as means  $\pm$  SE of three replicates (Student's *t*-test; \*\*,  $P < 0.01$ ).

(Cheng *et al.*, 2020; He *et al.*, 2021). However, the involvement of histone methylation modification in fleshy fruit ripening, a unique developmental process that Arabidopsis lacks, is poorly understood. Moreover, the interplay among different

epigenetic modifications to regulate gene expression is far from fully understood. Here, we have identified the histone H3K4 demethylase *SIJMJ7* as a negative regulator of tomato fruit ripening, and revealed a novel crosstalk axis between histone

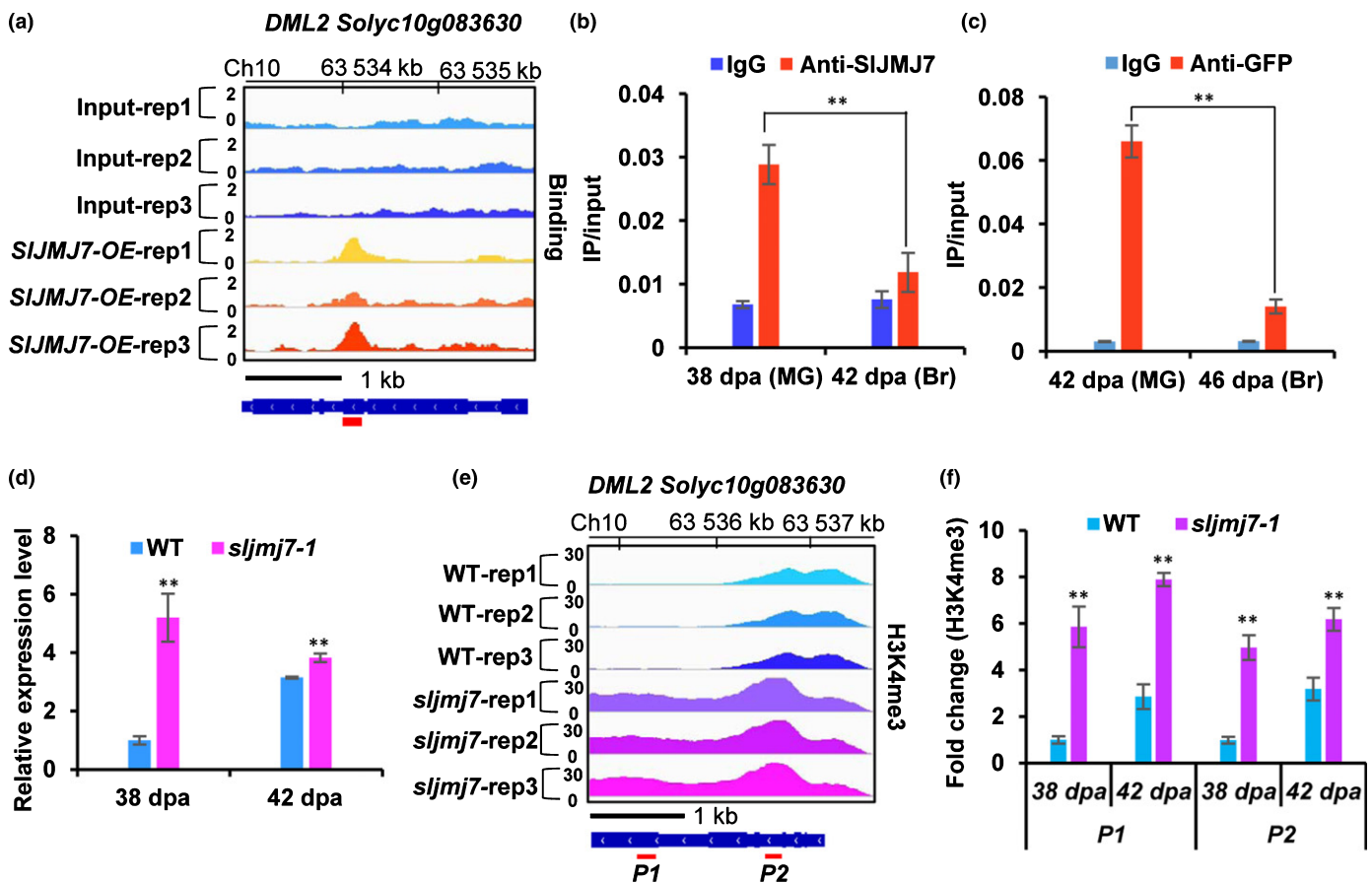


**Fig. 5** *SIJMJ7*-mediated removal of H3K4me3 represses the expression of *DML2* during fruit ripening in tomato. (a) Genome browser visualization of the binding sites of *SIJMJ7* in the DNA demethylase gene *DML2*, as detected by chromatin immunoprecipitation sequencing (ChIP-seq). (b) ChIP-quantitative PCR (ChIP-qPCR) analysis of the dynamic binding of *SIJMJ7* at the *DML2* gene in the WT fruits. Fruits of the WT plant at 38 d post-anthesis (dpa) were harvested for analysis. An anti-*SIJMJ7* antibody was used for immunoprecipitation, and immunoglobulin G (IgG) was used as the negative control. (c) ChIP-qPCR analysis of the dynamic binding of *SIJMJ7* at the *DML2* locus in *SIJMJ7-OE* fruits at 42 and 46 dpa. An anti-GFP antibody was used for immunoprecipitation, and IgG was used as the negative control. (d) Real-time quantitative polymerase chain reaction (RT-qPCR) analysis of the expression level of *DML2* in the WT and *sljmj7* mutant fruits at 38 and 42 dpa. *ACTIN* was used as the internal control. (e) Genome browser visualization of the H3K4me3 level at the *DML2* locus in the WT and *sljmj7-1* fruits. (f) ChIP-qPCR analysis of the H3K4me3 level in the WT and *sljmj7-1* fruits at 38 and 42 dpa. *ACTIN* was used as the internal control. In (a, e), gene structures are shown underneath. In (a), *P1* indicates the amplified regions by ChIP-qPCR in (b, c). In (e), *P1* and *P2* indicate the amplified regions by ChIP-qPCR in (f). All data are presented as means  $\pm$  SE of three replicates (Student's *t*-test; \*\*,  $P < 0.01$ ).

demethylation and DNA demethylation in the precise control of tomato fruit ripening. We have found that *SlJMj7* directly represses the expression of genes involved in regulating multiple crucial ripening processes, including ethylene biosynthesis, and genes encoding key ripening-related transcription factors,

via H3K4me3 demethylation. ChIP-seq analysis showed that mutation of *sljmj7* leads to a global increase in H3K4me3, confirming the role of *SlJMj7* in H3K4 demethylation. Moreover, *SlJMj7* binds to and represses *DML2*, a DNA demethylase required for fruit ripening, thus indirectly regulating the

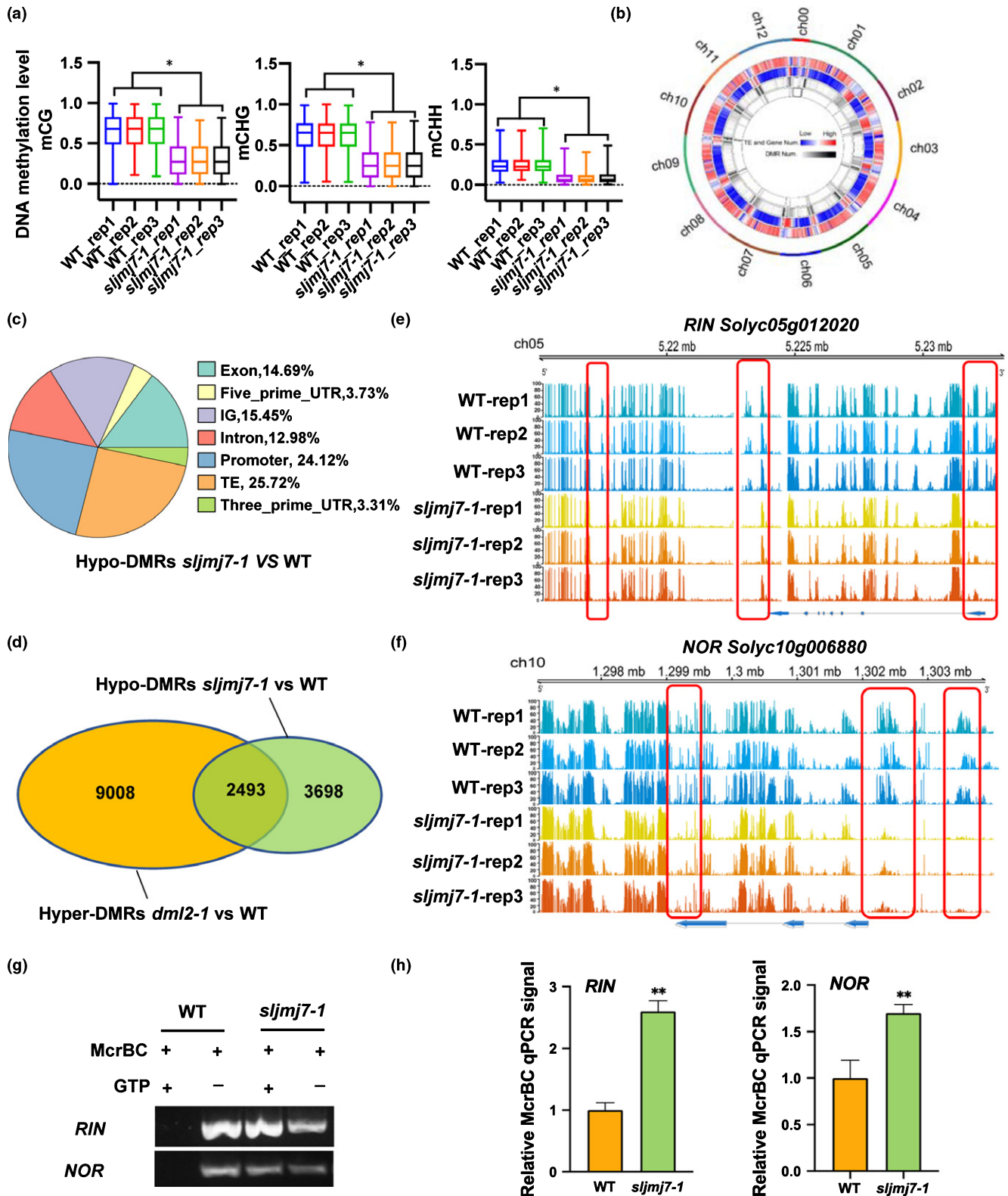


**Fig. 6** Loss of function of *SIJM7* causes genome-wide DNA hypomethylation in tomato fruits at 38 d post-anthesis (dpa) in tomato. (a) Boxplot analysis of the hypo-differentially methylated regions (hypo-DMRs) in the wild-type (WT) and *sljmj7-1* mutant fruits in three methylation contexts (CG, CHG and CHH). Centerlines show the medians; box limits indicate the 25<sup>th</sup> and 75<sup>th</sup> percentiles as determined by R software; whiskers extend 1.5 × interquartile range from the 25<sup>th</sup> and 75<sup>th</sup> percentiles. \*,  $P < 0.0001$  (unpaired *t*-test with Welch's correction). (b) Density plots of the transposable elements (TEs), genes and *sljmj7* hypo-DMRs on tomato chromosomes. (c) Distribution of the hypo-DMRs in the *sljmj7-1* mutant across different genomic regions. IG, intergenic region; UTR, untranslated region. (d) Venn diagram of the overlapping hypo-DMRs in *sljmj7-1* vs WT and hyper-DMRs in *dml2* vs WT in three contexts – CG, CHG, and CHH. The DMRs in each strain were compared with those in the WT. Hyper-DMRs, hyper-differentially methylated regions. (e, f) Genome browser visualization of the DNA methylation level of *RIN* (e) and *NOR* (f) in the WT and *sljmj7* mutant fruits, as determined by WGBS. The red boxes indicate the areas of hypomethylation of *RIN* and *NOR* in the *sljmj7* mutant compared with the WT. Three biological replicates were used. (g) DNA methylation levels of promoter regions of *RIN* and *NOR* in the WT and *sljmj7* mutant fruits by McrBC-PCR analysis. (h) DNA methylation levels of promoter regions of *RIN* and *NOR* in the WT and *sljmj7* mutant fruits by McrBC-qPCR analysis. Methylated DNA can be digested by McrBC restriction endonuclease, and thus higher qPCR signals indicate lower methylation levels. In (g, h), genomic DNA was digested overnight with McrBC, and the negative control for the digestion, which was performed without guanosine triphosphate (GTP), was used as the standard. dpa, days post-anthesis. The data are presented as the means ± SE of three replicates (Student's *t*-test; \*\*,  $P < 0.01$ ).

DNA methylome and ripening-related genes via DML2-mediated DNA demethylation.

Chromatin remodeling factors are crucial for the transcription regulation in plants; however, how these factors target the downstream genes remains unclear. Recent emerging evidence suggests that the JMJ protein REF6/AtJMJ12 may bind directly to their targets via three tandem ZnF motifs (Cui *et al.*, 2016; Li *et al.*, 2016). In addition to binding via direct recognition, JMJ proteins, such as AtJMJ30 and AtJMJ14, have been reported to be recruited to their targets via interaction with DNA-binding transcription factors, such as EFM, NAC050 and NAC052 (Yan *et al.*, 2014; Zhang *et al.*, 2015). Unlike REF6/AtJMJ12, the SIJM7 protein has no similar tandem ZnF DNA-binding domains, suggesting that SIJM7 may associate with its downstream genes via indirect manners. In the present work, SIJM7 is enriched in the binding motifs of a number of transcription factors, such as Bapx1 and TCX2. These findings suggest that SIJM7 may be recruited to its targets by interacting with transcription factors during tomato fruit ripening. However, further biochemical and physiological experiments are required to verify this hypothesis.

Histone methylation at H3K4 is usually related to gene activation and is reversibly regulated by histone H3K4 methyltransferases and demethylases (Berger, 2007). DNA methylation, which is established by *de novo* DNA methyltransferases and removed by DNA demethylases, is generally correlated with transcriptional inactivation (Law & Jacobsen, 2010). Crosstalk between DNA methylation and histone H3K4me3 demethylation has been previously reported in Arabidopsis. The histone H3K4me3 demethylase AtJMJ14 was found to be a component of the RNA-directed DNA methylation (RdDM) pathway (Deleris *et al.*, 2010; Searle *et al.*, 2010; Greenberg *et al.*, 2013). Mutations of *JMJ14* lead to decreased DNA methylation level at targets of domains rearranged methyltransferase 2-mediated RdDM, which is related to the increased H3K4me3 methylation. However, the direct interplay between H3K4me3 demethylation and DNA demethylation, and the underlying interaction mechanism are unknown in fleshy fruit ripening. Previously, repression or mutation of *DML2* has been shown to result in genome-wide hypermethylation and inhibition of fruit ripening in tomato (Liu *et al.*, 2015; Lang *et al.*, 2017). Here, we identified that *DML2* represents a direct target of SIJM7. Indeed, following the specific repression of *DML2* expression by SIJM7 via H3K4me3

demethylation at the MG stage, the protein abundance of SIJM7 decreases at the Br stage, and *DML2* expression is activated. Consistent with the early repression of *DML2* by SIJM7, loss of function of *SIJM7* caused a global DNA demethylation in tomato, resulting in accelerated fruit ripening. These findings demonstrate that SIJM7 regulates DNA methylation by specifically repressing *DML2* expression during fruit ripening. Moreover, the direct repression of *DML2* by SIJM7 in tomato fruit suggests a novel crosstalk axis between histone demethylation and DNA demethylation in plants. Previous studies have also supported the hypothesis that multiple types of epigenetic modifications may affect transcript stability. Zhou *et al.* (2019) reported that *DML2* transcript stability is modulated by N6-methyladenosine (m6A), revealing a direct interaction between DNA methylation and mRNA m<sup>6</sup>A methylation. Interestingly, our recent study showed that *DML2* is a target of SIJM6, a histone H3K27 demethylase, and SIJM6 activates the expression of *DML2* via removal of histone H3K27me3 (Z. Li *et al.*, 2020). Therefore, *DML2* might be a central target of multiple epigenetic modifications. A comprehensive analysis of the plant epigenome will help to illuminate how these epigenetic modifications combine to regulate the expression of *DML2* and its mediated DNA methylation.

In addition to the DNA methylation status, ethylene and key ripening-related transcription factors have been shown to be crucial regulators of fruit ripening in fleshy fruits (Wang *et al.*, 2020). In the present work, we showed that the expression of ethylene biosynthesis genes (*ACS2* and *ACS4*) was repressed by SIJM7-mediated removal of H3K4me3, indicating that SIJM7 plays an important role in modulating ethylene biosynthesis during tomato fruit ripening. Additionally, previous studies have shown that several transcription factors, including *RIN* and *NOR*, act as key ripening regulators in tomato. These regulators function upstream of both ethylene-dependent and ethylene-independent ripening pathways to regulate the expression of a large number of ripening-related genes (Vrebalov *et al.*, 2002; Manning *et al.*, 2006; Giovannoni, 2007; Qin *et al.*, 2012). The *rin* mutation causes fruit to fail to both produce elevated ethylene and respond to exogenous ethylene, and effectively block fruit ripening (Manning *et al.*, 2006). Interestingly, *DML2* activates the expression of *RIN*, *CNR* and *NOR* by demethylating the promoter regions of these genes (Liu *et al.*, 2015). Here, we found



## Author contributions

XDuan, XL and XDing conceived and designed the experiments. XDing performed most of the experiments, and GJ, ZL, YS and DZ performed the rest. XDuan, XDing, XL and YJ analyzed the data. XL and XDuan wrote the manuscript. XDing and XL contributed equally to this work.

## ORCID

Xuewu Duan  <https://orcid.org/0000-0002-9621-3865>  
 Yueming Jiang  <https://orcid.org/0000-0002-4648-9572>  
 Xuncheng Liu  <https://orcid.org/0000-0002-4098-5284>

## Data availability

The raw and processed RNA-seq and ChIP-seq (with the anti-GFP antibody and the anti-H3K4me3 antibody) data have been deposited in the NCBI GEO repository (<http://www.ncbi.nlm.nih.gov/geo>) under the accession no. GSE148527. The raw WGBS data have been deposited in NCBI GEO repository (GSE153080).

## References

- Berger SL. 2007. The complex language of chromatin regulation during transcription. *Nature* 447: 407–412.
- Cheng K, Xu Y, Yang C, Ouellette L, Niu L, Zhou X, Chu L, Zhuang F, Liu J, Wu H *et al.* 2020. Histone tales: lysine methylation, a protagonist in Arabidopsis development. *Journal of Experimental Botany* 71: 793–807.
- Cui X, Lu F, Qiu QI, Zhou B, Gu L, Zhang S, Kang Y, Cui X, Ma X, Yao Q *et al.* 2016. REF6 recognizes a specific DNA sequence to demethylate H3K27me3 and regulate organ boundary formation in Arabidopsis. *Nature Genetics* 48: 694–699.
- Deleris A, Greenberg MV, Ausin I, Law RW, Moissiard G, Schubert D, Jacobsen SE. 2010. Involvement of a Jumonji-C domain-containing histone demethylase in DRM2-mediated maintenance of DNA methylation. *EMBO Reports* 11: 950–955.
- Fillatti JJ, Kiser J, Rose R, Comai L. 1987. Efficient transfer of a glyphosate tolerance gene into tomato using a binary *Agrobacterium-tumefaciens* vector. *Nature Biotechnology* 5: 726–730.
- Gendrel AV, Lippman Z, Martienssen R, Colot V. 2005. Profiling histone modification patterns in plants using genomic tiling microarrays. *Nature Methods* 2: 213–218.
- Giovannoni J, Nguyen C, Ampofo B, Zhong S, Fei Z. 2017. The epigenome and transcriptional dynamics of fruit ripening. *Annual Review of Plant Biology* 68: 61–84.
- Giovannoni JJ. 2007. Fruit ripening mutants yield insights into ripening control. *Current Opinion in Plant Biology* 10: 283–289.
- Gray JE, Picton S, Giovannoni JJ, Grierson D. 1994. The use of transgenic and naturally-occurring mutants to understand and manipulate tomato fruit ripening. *Plant, Cell & Environment* 17: 557–571.
- Greenberg MVC, Deleris A, Hale CJ, Liu A, Feng SH, Jacobsen SE. 2013. Interplay between active chromatin marks and RNA-directed DNA methylation in *Arabidopsis thaliana*. *PLoS Genetics* 9: e1003946.
- Gu Z, Gu L, Eils R, Schlesner M, Brors B. 2014. CIRCLIZE Implements and enhances circular visualization in R. *Bioinformatics* 30: 2811–2812.
- Guo W, Fiziev P, Yan W, Cokus S, Sun X, Zhang MQ, Chen PY, Pellegrini M. 2013. BS-SEEKER2: a versatile aligning pipeline for bisulfite sequencing data. *BMC Genomics* 14: 774.
- Guo W, Zhu P, Pellegrini M, Zhang MQ, Wang X, Ni Z. 2018. CGMAPTools improves the precision of heterozygous SNV calls and supports allele-specific methylation detection and visualization in bisulfite-sequencing data. *Bioinformatics* 34: 381–387.
- He KX, Cao XF, Deng XA. 2021. Histone methylation in epigenetic regulation and temperature responses. *Current Opinion in Plant Biology* 61: 102001.
- He XJ, Chen T, Zhu JK. 2011. Regulation and function of DNA methylation in plants and animals. *Cell Research* 21: 442–465.
- Huang DW, Sherman BT, Lempicki RA. 2009. Systematic and integrative analysis of large gene lists using DAVID bioinformatics resources. *Nature Protocols* 4: 44–57.
- Huang H, Liu R, Niu Q, Tang K, Zhang B, Zhang H, Chen K, Zhu JK, Lang Z. 2019. Global increase in DNA methylation during orange fruit development and ripening. *Proceedings of the National Academy of Sciences, USA* 116: 1430–1436.
- Huang S, Zhang A, Jin JB, Zhao B, Wang TJ, Wu Y, Wang S, Liu Y, Wang J, Guo P *et al.* 2019. Arabidopsis histone H3K4 demethylase JM17 functions in dehydration stress response. *New Phytologist* 223: 1372–1387.
- Klose RJ, Zhang Y. 2007. Regulation of histone methylation by demethylination and demethylation. *Nature Reviews Molecular Cell Biology* 8: 307–318.
- Kouzarides T. 2007. Chromatin modifications and their function. *Cell* 128: 693–705.
- Lang Z, Wang Y, Tang K, Tang D, Datsenka T, Cheng J, Zhang Y, Handa AK, Zhu JK. 2017. Critical roles of DNA demethylation in the activation of ripening-induced genes and inhibition of ripening-repressed genes in tomato fruit. *Proceedings of the National Academy of Sciences, USA* 114: E4511–E4519.
- Law JA, Jacobsen SE. 2010. Establishing, maintaining and modifying DNA methylation patterns in plants and animals. *Nature Reviews Genetics* 11: 204–220.
- Le Masson I, Jauvion V, Bouteiller N, Rivard M, Elmayan T, Vaucheret H. 2012. Mutations in the Arabidopsis H3K4me2/3 demethylase JM14 suppress posttranscriptional gene silencing by decreasing transgene transcription. *Plant Cell* 24: 3603–3612.
- Li C, Gu L, Gao L, Chen C, Wei C-Q, Qiu QI, Chien C-W, Wang S, Jiang L, Ai L-F *et al.* 2016. Concerted genomic targeting of H3K27 demethylase REF6 and chromatin-remodeling ATPase BRM in Arabidopsis. *Nature Genetics* 48: 687–693.
- Li D, Liu RY, Singh D, Yuan XY, Kachroo P, Raina R. 2020. JM14 encoded H3K4 demethylase modulates immune responses by regulating defence gene expression and piperolic acid levels. *New Phytologist* 225: 2108–2121.
- Li Z, Jiang G, Liu X, Ding X, Zhang D, Wang X, Zhou Y, Yan H, Li T, Wu K *et al.* 2020. Histone demethylase SLMJ6 promotes fruit ripening by removing H3K27 methylation of ripening-related genes in tomato. *New Phytologist* 227: 1138–1156.
- Liang QI, Deng H, Li Y, Liu Z, Shu P, Fu R, Zhang Y, Pirrello J, Zhang Y, Grierson D *et al.* 2020. Like heterochromatin protein 1b represses fruit ripening via regulating the H3K27me3 levels in ripening-related genes in tomato. *New Phytologist* 227: 485–497.
- Liu CY, Lu FL, Cui X, Cao XF. 2010. Histone methylation in higher plants. *Annual Review of Plant Biology* 61: 395–420.
- Liu H, Ding YD, Zhou YQ, Jin WQ, Xie KB, Chen LL. 2017. CRISPR-P 2.0: an improved CRISPR-Cas9 tool for genome editing in plants. *Molecular Plant* 10: 530–532.
- Liu P, Zhang S, Zhou B, Luo XI, Zhou XF, Cai B, Jin YH, Niu DE, Lin J, Cao X *et al.* 2019. The histone H3K4 demethylase JM16 represses leaf senescence in Arabidopsis. *Plant Cell* 31: 430–443.
- Liu R, How-Kit A, Stammitt L, Teyssier E, Rolin D, Mortain-Bertrand A, Halle S, Liu M, Kong J, Wu C *et al.* 2015. A DEMETER-like DNA demethylase governs tomato fruit ripening. *Proceedings of the National Academy of Sciences, USA* 112: 10804–10809.
- Lu F, Li G, Cui X, Liu C, Wang XJ, Cao X. 2008. Comparative analysis of JmjC domain-containing proteins reveals the potential histone demethylases in Arabidopsis and rice. *Journal of Integrative Plant Biology* 50: 886–896.
- Lu FL, Cui X, Zhang SB, Jenuwein T, Cao XF. 2011. Arabidopsis REF6 is a histone H3 lysine 27 demethylase. *Nature Genetics* 43: 715–719.
- Lu FL, Cui X, Zhang SB, Liu CY, Cao XF. 2010. JM14 is an H3K4 demethylase regulating flowering time in Arabidopsis. *Cell Research* 20: 387–390.

- Manning K, Tor M, Poole M, Hong Y, Thompson AJ, King GJ, Giovannoni JJ, Seymour GB. 2006. A naturally occurring epigenetic mutation in a gene encoding an SBP-box transcription factor inhibits tomato fruit ripening. *Nature Genetics* 38: 948–952.
- Mosammaparast N, Shi Y. 2010. Reversal of histone methylation: biochemical and molecular mechanisms of histone demethylases. *Annual Review of Biochemistry* 79: 155–179.
- Qin GZ, Wang YY, Cao BH, Wang WH, Tian SP. 2012. Unraveling the regulatory network of the MADS box transcription factor RIN in fruit ripening. *The Plant Journal* 70: 243–255.
- Ricardi MM, Gonzalez RM, Iusem ND. 2010. Protocol: fine-tuning of a chromatin immunoprecipitation (ChIP) protocol in tomato. *Plant Methods* 6: 11.
- Searle IR, Pontes O, Melnyk CW, Smith LM, Baulcombe DC. 2010. JMj14, a JmjC domain protein, is required for RNA silencing and cell-to-cell movement of an RNA silencing signal in Arabidopsis. *Genes & Development* 24: 986–991.
- Seymour GB, Chapman NH, Chew BL, Rose JKC. 2013. Regulation of ripening and opportunities for control in tomato and other fruits. *Plant Biotechnology Journal* 11: 269–278.
- Shi Y, Lan F, Matson C, Mulligan P, Whetstone JR, Cole PA, Casero RA, Shi Y. 2004. Histone demethylation mediated by the nuclear amine oxidase homolog LSD1. *Cell* 119: 941–953.
- Song QX, Huang TY, Yu HH, Ando A, Mas P, Ha M, Chen ZJ. 2019. Diurnal regulation of SDG2 and JMj14 by circadian clock oscillators orchestrates histone modification rhythms in Arabidopsis. *Genome Biology* 20: 170.
- Thompson AJ, Tor M, Barry CS, Vrebalov J, Orfila C, Jarvis MC, Giovannoni JJ, Grierson D, Seymour GB. 1999. Molecular and genetic characterization of a novel pleiotropic tomato-ripening mutant. *Plant Physiology* 120: 383–390.
- Tsukada Y, Fang J, Erdjument-Bromage H, Warren ME, Borchers CH, Tempst P, Zhang Y. 2006. Histone demethylation by a family of JmjC domain-containing proteins. *Nature* 439: 811–816.
- Vrebalov J, Ruzinsky D, Padmanabhan V, White R, Medrano D, Drake R, Schuch W, Giovannoni J. 2002. A MADS-box gene necessary for fruit ripening at the tomato ripening-inhibitor (*rin*) locus. *Science* 296: 343–346.
- Wang R, Angenent GC, Seymour G, de Maagd RA. 2020. Revisiting the role of master regulators in tomato ripening. *Trends in Plant Science* 25: 291–301.
- Wang TJ, Huang S, Zhang A, Guo P, Liu Y, Xu C, Cong W, Liu B, Xu ZY. 2021. JMj17-WRKY40 and HY5-ABI5 modules regulate the expression of ABA-responsive genes in Arabidopsis. *New Phytologist* 230: 567–584.
- Wang ZP, Wang SB, Li DW, Zhang Q, Li L, Zhong CH, Liu YF, Huang HW. 2018. Optimized paired-sgRNA/Cas9 cloning and expression cassette triggers high-efficiency multiplex genome editing in kiwifruit. *Plant Biotechnology Journal* 16: 1424–1433.
- Xu CJ, Fraser PD, Wang WJ, Bramley PM. 2006. Differences in the carotenoid content of ordinary citrus and lycopene-accumulating mutants. *Journal of Agricultural and Food Chemistry* 54: 5474–5481.
- Yan Y, Shen L, Chen Y, Bao S, Thong Z, Yu H. 2014. A MYB-domain protein EFM mediates flowering responses to environmental cues in Arabidopsis. *Developmental Cell* 30: 437–448.
- Zhang S, Zhou B, Kang Y, Cui X, Liu AO, Deleris A, Greenberg MVC, Cui X, Qiu QI, Lu F *et al.* 2015. C-terminal domains of histone demethylase JMj14 interact with a pair of NAC transcription factors to mediate specific chromatin association. *Cell Discovery* 1: 15003.
- Zheng X, Xie Z, Zhu K, Xu Q, Deng X, Pan Z. 2015. Isolation and characterization of carotenoid cleavage dioxygenase 4 genes from different citrus species. *Molecular Genetics and Genomics* 290: 1589–1603.
- Zhong S, Fei Z, Chen Y-R, Zheng YI, Huang M, Vrebalov J, McQuinn R, Gapper N, Liu B, Xiang J *et al.* 2013. Single-base resolution methylomes of tomato fruit development reveal epigenome modifications associated with ripening. *Nature Biotechnology* 31: 154–159.
- Zhou L, Tian S, Qin G. 2019. RNA methylomes reveal the m(6)A-mediated regulation of DNA demethylase gene SIDML2 in tomato fruit ripening. *Genome Biology* 20: 156.

## Supporting Information

Additional Supporting Information may be found online in the Supporting Information section at the end of the article.

**Dataset S1** Primer pairs used in this study.

**Dataset S2** List of upregulated genes in *sljmj7-1* mutant.

**Dataset S3** List of downregulated genes in *sljmj7-1* mutant.

**Dataset S4** List of SIJMj7-bound sites.

**Dataset S5** List of genes with increased level of H3K4me3 in *sljmj7-1* mutant.

**Dataset S6** List of SIJMj7-repressed and -bound genes which are regulated by H3K4me3.

**Dataset S7** Mapping statistics of WGBS libraries.

**Dataset S8** Hypo-CG-DMRs in *sljmj7-1* mutant.

**Dataset S9** Hypo-CHG-DMRs in *sljmj7-1* mutant.

**Dataset S10** Hypo-CHH-DMRs in *sljmj7-1* mutant.

**Dataset S11** Hyper-CG-DMRs in *sljmj7-1* mutant.

**Dataset S12** Hyper-CHG-DMRs in *sljmj7-1* mutant.

**Dataset S13** Hyper-CHH-DMRs in *sljmj7-1* mutant.

**Dataset S14** Overlap of hypo-DMRs in *sljmj7* and hyper-DMRs in *dml2*.

**Dataset S15** Hypo-CG-DMRs of fruit ripening-related genes in *sljmj7-1* vs WT.

**Dataset S16** Hypo-CHG-DMRs of fruit ripening-related genes in *sljmj7-1* vs WT.

**Dataset S17** Hypo-CHH-DMRs of fruit ripening-related genes in *sljmj7-1* vs WT.

**Fig. S1** Phylogenetic analysis of KDM5/JARIDA1 group proteins in Arabidopsis and tomato.

**Fig. S2** Construction and identification of *sljmj7* knockout mutants in tomato.

**Fig. S3** Detection of H3K9 demethylase activity of SIJMj7 protein in tobacco leaves by immunofluorescence assay.

**Fig. S4** Detection of H3K27 demethylase activity of SIJMj7 protein in tobacco leaves by immunofluorescence assay.

**Fig. S5** Detection of H3K36 demethylase activity of SlJM7 protein in tobacco leaves by immunofluorescence assay.

**Fig. S6** Architecture domains of KDM5/JARID1 group proteins.

**Fig. S7** Validation of RNA-seq results by RT-qPCR in tomato.

**Fig. S8** Distribution of the SlJM7 binding sites in tomato genome.

**Fig. S9** Gene browser view of the binding sites and H3K4me3 level of flavonoid/anthocyanin biosynthesis genes *CHS1* and *LoxC* and carotenoid biosynthesis genes *PSY1* and *ZISO* detected by ChIP-seq assay in tomato.

**Fig. S10** Verification of the binding sites of SlJM7 in ripening-related genes by ChIP-qPCR assay in tomato.

**Fig. S11** ChIP-qPCR analysis of the histone H3K4me3 level of ripening-related genes in WT and *sljm7* mutant.

**Fig. S12** Distribution of the hyper-DMRs in the *sljm7-1* mutant across different genomic regions.

**Fig. S13** Gene browser view of DNA methylation level of *ACS2*, *ACS4*, *PSY1*, *CNR*, *ACS8*, *ACO2*, *AP2a*, *PL*, *PME1.9* and *TBG4* and *sljm7* mutant fruits as detected by ChIP-seq assay.

Please note: Wiley Blackwell are not responsible for the content or functionality of any Supporting Information supplied by the authors. Any queries (other than missing material) should be directed to the *New Phytologist* Central Office.



## About *New Phytologist*

- *New Phytologist* is an electronic (online-only) journal owned by the New Phytologist Foundation, a **not-for-profit organization** dedicated to the promotion of plant science, facilitating projects from symposia to free access for our Tansley reviews and Tansley insights.
- Regular papers, Letters, Viewpoints, Research reviews, Rapid reports and both Modelling/Theory and Methods papers are encouraged. We are committed to rapid processing, from online submission through to publication 'as ready' via *Early View* – our average time to decision is <26 days. There are **no page or colour charges** and a PDF version will be provided for each article.
- The journal is available online at Wiley Online Library. Visit **www.newphytologist.com** to search the articles and register for table of contents email alerts.
- If you have any questions, do get in touch with Central Office (np-centraloffice@lancaster.ac.uk) or, if it is more convenient, our USA Office (np-usaoffice@lancaster.ac.uk)
- For submission instructions, subscription and all the latest information visit **www.newphytologist.com**